2011 9th IEEE International Conference on
Control and Automation (ICCA)
Santiago, Chile, December 19-21, 2011

High-Bandwidth Control Design for a Piezoelectric Nanopositioning Stage

Jinchuan Zheng and Minyue Fu

Abstract— **To achieve fast and accurate tracking of a wideband reference trajectory, the piezoelectric (PZT) actuator requires a high-bandwidth control system, which is however restricted by the resonant mode of the PZT positioning stage. In this paper, we study two resonant compensation techniques to damp the resonant mode for increased servo bandwidth. First, we present a feedback control system using a conventional notch filter (NF). Subsequently, we develop a complex lead compensator (CLC) using the phase-stabilized compensation method. Unlike the NF that is aimed at reducing the resonant peak gain, the CLC specializes in shaping the phase of open-loop system at the resonant frequency. The analysis shows that the closed-loop bandwidth achieved by the CLC is around four times higher than that of the NF without sacrificing the stability margin. Finally, we propose a multi-resonant filter (MRF) to suppress periodic tracking errors by significantly attenuating the gains at specified frequencies in the sensitivity function. The experimental results verify that the CLC is superior in disturbance compensation and periodic trajectory tracking as compared to the NF, and the add-on MRF can greatly reduce the tracking error.**

I. Introduction

The piezoelectric (PZT) nanopositioning stages are widely used in industrial applications such as atomic force microscope (AFM) [1]. The PZT actuator can produce extremely small displacements in the range of subnanometer to a few hundreds micrometers with nanoscale positioning precision. Feedback controllers are typically used to compensate for the nonlinear PZT hysteresis and creep effect, and the mechanical resonant mode and to obtain a high servo bandwidth for robust and accurate tracking of a wideband reference trajectory. A thorough literature review on control approaches for PZT actuators is reported in [2]. For vibration control, the main approach is to damp the resonant mode. This has been done by several design methods such as the notch filter (NF) [3] and the integral resonant control [4]. The resonant compensator resulted from these design methods is low-order and thus easy to implement. In this paper, we develop an alternative resonant compensator named as complex lead compensator (CLC) to damp the resonant mode. Unlike the notch filter that is aimed at reducing the open-loop gain at the resonant peak, the CLC changes the open-loop phase characteristics at the resonant frequency such that the resonant mode is not significantly excited by the reference commands or the input disturbances during closed-loop operations. Moreover, it is shown that the CLC can lead to a higher closed-loop bandwidth than that of the NF without sacrificing the stability margin, resulting in more accurate tracking of a wideband reference trajectory.

Tracking control is another control task for the PZT actuators to drive the position output to track a desired trajectory for specific applications. For example, in AFM applications, the most common form of trajectory is to use a triangular waveform in the X-axis and a linear ramp in the Y-axis, thus the combination of which in both axes achieves the desired raster scan motion [5]. Moreover, in manufacturing applications such as nanoassembly [6] and power sintering process [7], step reference is used for fast positioning such as in pick-and-place operations. To achieve these tasks, traditional proportional-integral-derivative (PID) controllers are widely used (see e.g., [7], [8]); and higher-order controllers designed with modern control technologies are also reported such as repetitive control [9]. In this paper, we develop a design method by using a multi-resonant filter (MRF) to achieve desired narrow-band gain attenuations at specified frequencies in the sensitivity function without destabilizing the control system. This method can be applied to achieve precise tracking of periodic trajectories by simply adding the MRF whose attenuation frequencies are placed at the harmonics frequencies of the periodic trajectory.

II. Plant Modeling

Fig. 1 shows the experimental setup of the PZT nanopositioning stage (P-752, Polytec PI) studied in this paper. It consists of a flexure-guided moving stage that is driven by a PZT microactuator with a travel range of 25 μm, and a capacitive position sensor with a practical resolution of 9 nm to measure the displacement of the moving stage along the axis. The position sensor output is fedback to a real-time DSP system (dSPACE-DS1103) on which the feedback controller is implemented with the sampling frequency of 20 kHz. Subsequently, the control signal is passed through the PZT voltage amplifier (E-505, Polytec PI) to drive the PZT actuator.

The system dynamics of the PZT nanopositioning stage contain the nonlinear PZT hysteresis effect and the linear model associated with the vibrational dynamics. In our study, the nonlinear hysteresis is regarded as a bounded input disturbance to the PZT actuator. The frequency response data from the PZT control input signal u to the displacement output y [the measured PZT plant model $P(s)$] was obtained and plotted by the dashed lines in Fig. 2. We can see that the PZT linear dynamics are dominated by two resonance modes in the measured frequency range of interest. The

J. Zheng and M. Fu are with the School of Electrical Engineering and Computer Science, The University of Newcastle, Callaghan, NSW 2308, Australia. Jinchuan.Zheng@newcastle.edu.au; Minyue.Fu@newcastle.edu.au

978-1-4577-1476-4/11/$26.00 ©2011 IEEE

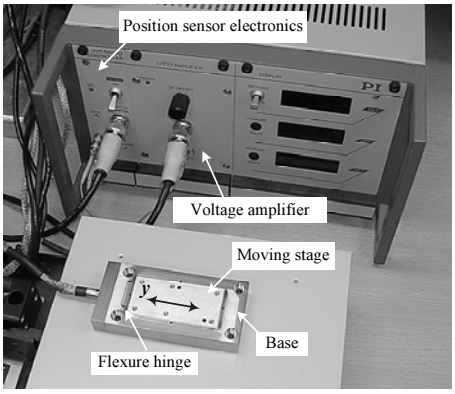

Fig. 1. Experimental setup of the PZT nanopositioning stage.

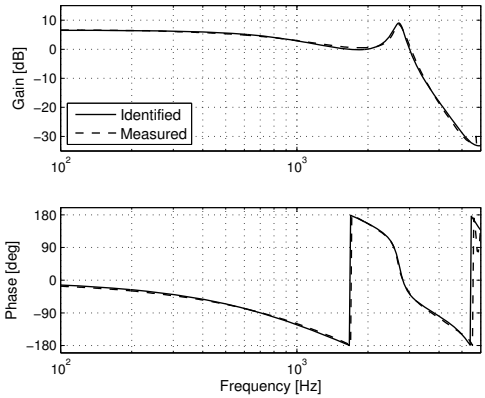

Fig. 2. Frequency responses of the linear PZT model $P(s)$.

first mode that has a large damping ratio (as the resonant peak is insignificant at the resonant frequency 1018 Hz) is caused by the voltage amplifier due to the capacitive load presented by the PZT actuator. The second mode has a relatively large resonant peak (10 dB) at 2721 Hz, which is caused by the flexibility of the flexure hinge. We note that the first mode is associated with 180° phase drop, which significantly decreases the phase margin, resulting in a limited servo bandwidth. Moreover, the second mode may induce significant vibrations to the stage motion and should be carefully damped.

By using the complex curve-fitting algorithm [10], a 4th-order transfer function is identified for the PZT as follows

$$P(s) = 0.0514 \cdot \frac{s^2 - 29668s + 3.914 \times 10^8}{s^2 + 11290s + 4.085 \times 10^7} \cdot \frac{s^2 - 11380s + 1.263 \times 10^9}{s^2 + 1730s + 2.919 \times 10^8} \quad (\frac{\mu\text{m}}{V}). \tag{1}$$

The solid lines in Fig. 2 indicate that the identified model has a close match with the measured model.

III. High-Bandwidth Feedback Controller Designs

In this section, we develop two resonant compensators based on the feedback control structure to achieve high servo bandwidth for the PZT nanopositioning stage. First, the feedback control structure based on integral control is described. Subsequently, the well-known notch filter servo control is shown. Next, we present a complex lead compensator design method for increased servo bandwidth. Finally, experimental results are shown to verify the effectiveness of the designed controllers.

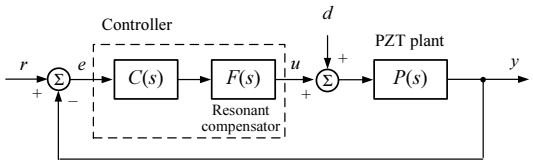

Fig. 3. Block diagram of the PZT feedback control structure, where $C(s)$ is the integral controller, $F(s)$ is the resonant compensator, r is the reference trajectory, y the output displacement, e the tracking error, and u the control input. d represents the lumped nonlinear hysteresis effect and input disturbance.

A. Control Structure

The block diagram of the PZT feedback control structure is shown in Fig. 3, where $C(s)$ is an integral controller to achieve high-gain feedback control, which is given by

$$C(s) = \frac{k_i}{s}, \tag{2}$$

where k_i is the integral gain. The controller $F(s)$ is the resonant compensator, which is obtained by different design techniques as will be shown later. The control objective here is to achieve the maximum closed-loop servo bandwidth, and guarantee the minimal stability margin, that is, phase margin $> 40^\circ$, and gain margin > 6 dB.

B. Notch Filter Servo Control

First, we design the resonant compensator $F(s)$ in Fig. 3 using the conventional notch filter, which is given by

$$F_{nf}(s) = \frac{s^2 + 2\zeta_{n2}\omega_n s + \omega_n^2}{s^2 + 2\zeta_{n1}\omega_n s + \omega_n^2}, \tag{3}$$

where $\omega_n = 2\pi 2721$, $\zeta_{n1} = 0.3$, and $\zeta_{n2} = 0.04$. Moreover, the integral controller gain of (2) is maximized to be $k_i = 1000$ subject to the required stability margin.

The frequency response functions (FRFs) of the notch filter based control system is shown in Fig. 4. We can see that the notch filter significantly reduces the gain of the second resonance peak at 2721 Hz. However, the associated phase lag of the notch filter decreases the phase margin. Thus, the closed-loop bandwidth cannot be greatly increased for the sake of maintaining the desired phase margin.

C. Complex Lead Compensator Servo Control

In our particular case, we observe that the first resonance mode caused by the voltage amplifier has a large damping ratio of 0.9; and additionally its resonance frequency at 1018 Hz is inherently not sensitive to the load variations which are considered as the major uncertainties in our study. This means that the first resonance mode is relatively stable

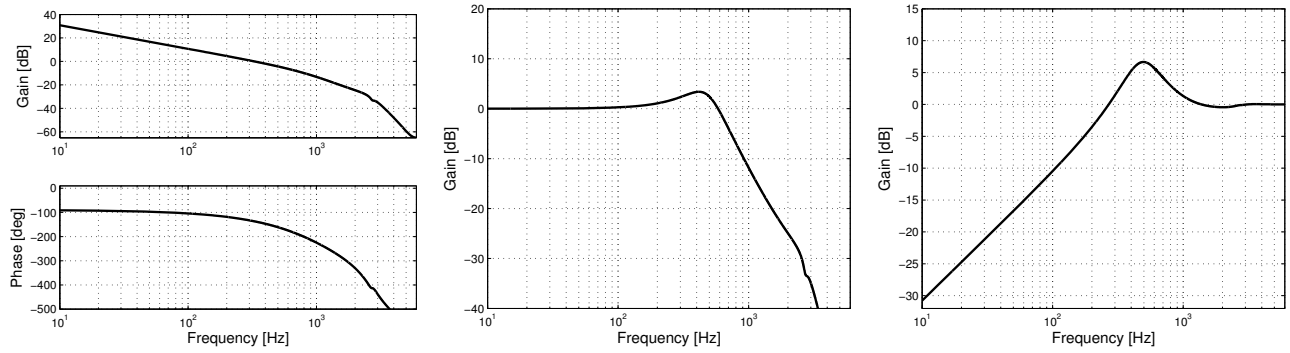

(a) (b) (c)

Fig. 4. Frequency response of notch filter based control system. (a) Open-loop FRF $= PCF_{nf}$. The notch filter decreases the gain of the resonance peak at 2721 Hz and results in phase margin $= 43\,^{\circ}$, gain margin $= 7.04$ dB; (b) Closed-loop FRF $= PCF_{nf}/(1+PCF_{nf})$. The maximum bandwidth achievable is 630 Hz; (c) Sensitivity FRF $= 1/(1+PCF_{nf})$. The gain of the resonance peak at 2721 Hz is damped to 0 dB.

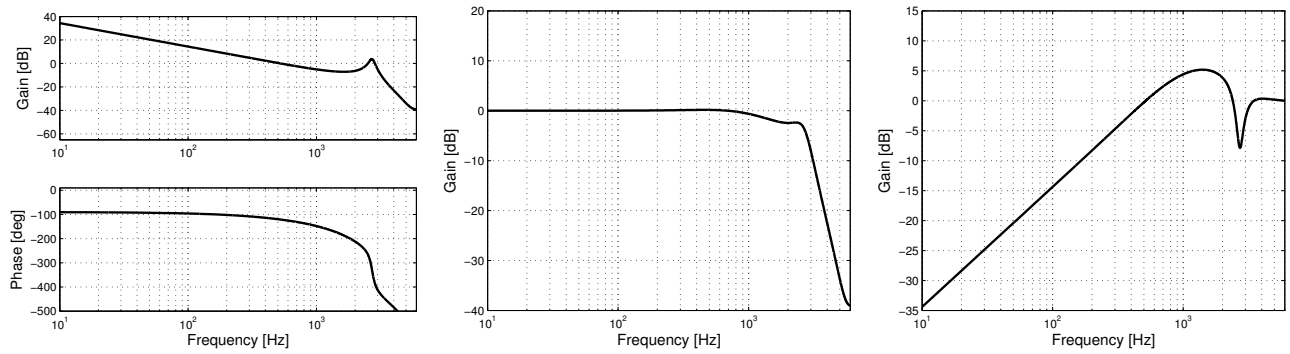

(a) (b) (c)

Fig. 5. Frequency response of complex lead compensator based control system. (a) Open-loop FRF $= PCF_{\,clc}$. The complex lead compensator not only cancels the first resonance mode but also phase-stabilizes the second resonance mode. The phase margin $= 58\,^{\circ}$, gain margin $= 7.0$ dB, and the phase at the second resonance frequency is shaped as $-360\,^{\circ} + 25^{\circ}$@2721 Hz; (b) Closed-loop FRF $= PCF_{clc}/(1+PCF_{clc})$. The maximum bandwidth achievable is significantly increased to be 2512 Hz; (c) Sensitivity FRF $= 1/(1+PCF_{clc})$. The gain of the resonance peak at 2721 Hz is further damped to -8 dB; and the gains at low frequencies are also smaller than those in Fig. 4(c), implying higher disturbance rejection capability.

compared to the second resonance mode that is sensitivity to the load variations.

Hence, it is feasible to use a complex lead compensator whose zeros are set to cancel the poles of the first resonance mode. In this way, the gain roll-off and phase lag due to the first resonance mode are completely compensated; and thus a larger integral gain can be applied to increase the bandwidth without sacrificing the stability margin. However, the complex lead compensator inversely produces the problem of increasing the gain of the second resonance peak. It is interesting to find that the second resonance mode can be compensated simultaneously using the phase-stabilized control method [11]. More specifically, the poles of the complex lead compensator should be designed to secure the phase of the second resonance peak within $-360^{\circ} \pm 90^{\circ}$ in the open-loop system. Note that this method differs from the notch filter that dedicates to the gain reduction of the resonance peak. The complex lead compensator is given by

$$F_{clc}(s) = \frac{w_p}{w_z} \cdot \frac{s^2 + 2\zeta_{clc}\omega_z s + \omega_z^2}{s^2 + 2\zeta_{clc}\omega_p s + \omega_p^2}, \tag{4}$$

where $\omega_z = 2\pi 1015$, $\omega_p = 2\pi 4000$, and $\zeta_{clc} = 0.85$. Moreover, a larger integral controller gain $k_i = 6100$ in (2) is now applicable subject to the required stability margin. Note that compared to the lead compensator with real poles and zeros that offers the equal maximum phase lead, the complex lead compensator in (4) has a smaller ratio of the high-frequency gain asymptote to the low-frequency gain asymptote [12]. This property can avoid the amplification of the high-frequency portion of the sensor noise.

The frequency response functions of the complex lead compensator based control system is shown in Fig. 5. The obtained specifications of the control system with NF and CLC will be summarized later in Table II, which indicates

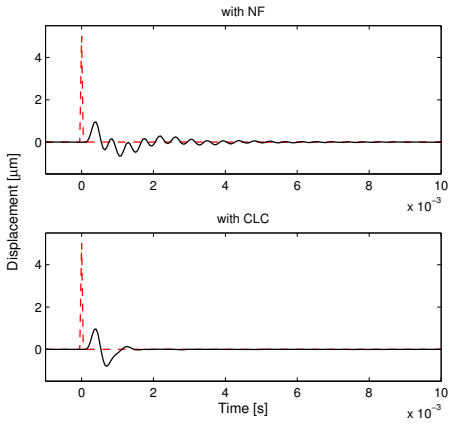

Fig. 6. Impulse response. Dashed lines: 5 V impulse input disturbance d; Solid lines: output displacement y. The NF based control excites the second resonance mode. The CLC based control does not excite the resonance mode, resulting in faster settling time.

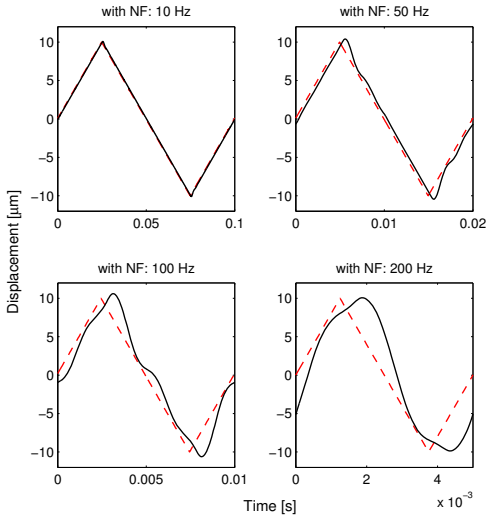

Fig. 7. Triangular waveform tracking with notch filter control. Dashed lines: Triangular reference; Solids lines: Output displacement.

that the CLC can achieve a four times higher closed-loop bandwidth while satisfying the required stability margin.

D. Experimental Results

The above designed notch filter and complex lead compensator are implemented on the PZT nanopositioning stage, respectively. First, Fig. 6 shows the experimental result of impulse input disturbance rejection (by artifically injecting a 5 V impulse to the control input). We can see that the CLC control does not excite the resonance mode. The result verifies the sensitivity FRFs as shown in Figs. 4(c) and 5(c), from which the notched gains at the second resonant frequency implies less resonance excitation. Secondly, we compare the triangular waveform tracking in Figs. 7 and 8, respectively. It is clear that the CLC has smaller tracking errors than those of NF in all cases of reference frequencies. Detail performance index will be summarized later in Table III.

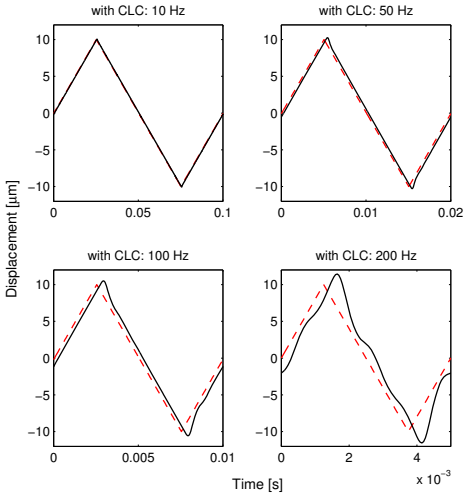

Fig. 8. Triangular waveform tracking with complex lead compensator control. Dashed lines: Triangular reference; Solids lines: Output displacement.

IV. Multi-Resonant Filter Design For Improved Periodic Tracking Control

In this section, we develop an add-on multi-resonant filter for improved periodic tracking performance. Experimental results are presented to demonstrate the significant improvement of the tracking performance when the MRF is added on the baseline control system.

A. Design Concept

Fig. 9 shows the block diagram of the MRF, which is connected in parallel with the baseline controller for easy implementation. The baseline control system is assumed to have basic stability margin and performance.

The design criteria here is to shape the gains of the sensitivity function at the harmonics frequencies of the periodic reference trajectories as small as possible. As a result, the tracking error $e(t) = r(t) - y(t)$ will be reduced for a given $r(t)$. More specifically, from Fig. 9, we can derive the sensitivity function from the tracking error $e(t)$ to the reference signal $r(t)$ as follows

$$\begin{aligned} S(s) = \frac{e}{r} &= \frac{1}{1+PCF(1+M)} \\ &= \frac{1}{1+PCF} \cdot \frac{1}{1+T_0 M} \\ &= S_0 \cdot S_M \end{aligned} \tag{5}$$

where

$$T_0 = \frac{PCF}{1+PCF} \tag{6}$$

Note that S_0 and T_0 are the sensitivity function and the closed-loop function of the baseline control system, respectively. The equation (5) shows that the overall sensitivity function $S(s)$ is the multiplication of two subsystem S_0 and S_M, which implies that the multi-resonant filter $M(s)$ can be designed based on the pseudo-plant T_0 such that S_M is shaped to a desired curve for reducing the tracking error within some frequency ranges provided S_M is stable [13].

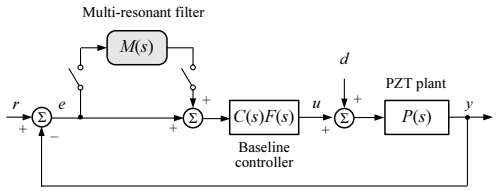

Fig. 9. Block diagram of the PZT control system using an add-on multi-resonant filter with parallel connection with the baseline controller.

TABLE I
PARAMETERS OF THE MULTI-RESONANT FILTER

i	ω_i (rad/s)	φ_i	ζ_i	m_i
1	$2\pi 200$	-0.385	3.98×10^{-4}	0.25
2	$2\pi 600$	-1.215	1.33×10^{-4}	0.026
3	$2\pi 1000$	-2.068	1.19×10^{-4}	3.88×10^{-4}
4	$2\pi 1400$	-2.883	5.68×10^{-5}	1.06×10^{-4}

To provide narrow-band high gains at the harmonics frequencies of the periodic reference trajectory, the MRF with the following form is used

$$M(s) = \sum_{i=1}^{n} m_i \frac{s[\omega_i \cos(\varphi_i) - \sin(\varphi_i)s]}{s^2 + 2\zeta_i\omega_i s + \omega_i^2}, \tag{7}$$

where n is the number of the harmonics, ω_i is the harmonics frequency of the reference trajectory, ζ_i is the damping ratio with $\zeta_i \in (0, 1)$, m_i is a positive gain, and φ_i is the phase angle determined by

$$\varphi_i = \arg\left[T_0(j\omega_i)\right] \in [-\pi, \pi]. \tag{8}$$

Note that the key feature of the MRF of (7) lies in that the filter zeros are specifically placed at 0 and $\omega_i \text{ctan}(\varphi_i)$, which can lead to slight influence of the stability margin for a tiny m_i, and additionally achieve minimal sensitivity gains at the harmonics frequencies (see our analysis results in [13]). Now we give the formulae of m_i and ζ_i, which are explicitly expressed by the design specifications ζ_i and D_i as illustrated in Fig. 11(c),

$$\zeta_i = \frac{\Delta_i(\omega_i + 0.5\Delta_i)}{4\omega_i^2}, \tag{9}$$

$$m_i = (10^{D_i/20} - 1)\frac{2\zeta_i}{|T_0(j\omega_i)|}, \tag{10}$$

where Δ_i is the frequency difference between the two points which are approximately $0.3D_i$ away from the notch at the harmonics frequency ω_i, and D_i (unit: dB) is the desired reduction ratio at ω_i. Note that choosing too large Δ_i or D_i may destabilize the control system; in contrast, reducing Δ_i or D_i diminishes the effect of the MRF.

For demonstration of the design, we suppose the baseline controller is the feedback controller with the CLC as designed in Section III.C and the triangular waveform is of fundamental frequency of 200 Hz. Then, the MRF can be easily obtained according the above results. We choose $n = 4$ to further compensate for the first 4 odd harmonics of the triangular waveform. The designed MRF parameters are listed in Table I and the frequency response of the resulting overall controller $CF_{clc}(1 + M)$ is shown in Fig. 10.

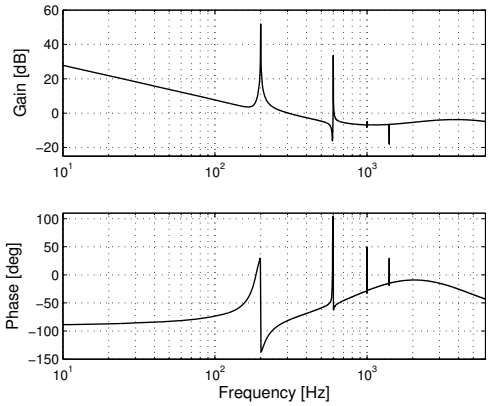

Fig. 10. Frequency response of the feedback controller $CF_{clc}(1 + M)$.

The frequency response functions of the control system with the CLC/MRF is shown in Fig. 11, which indicates that the stability margin is almost maintained and the MRF further reduces the sensitivity gains at the first 4 odd harmonics frequencies of the triangular waveform. Table II summarizes the specifications of the developed controllers. We can see that the CLC/MRF control achieves the highest closed-loop bandwidth with the desired stability margin.

B. Experimental Result

The MRF is implemented by simply plugging into the CLC control system and the experimental results of triangular waveform tracking is shown in Fig. 12. It is clear that the MRF greatly reduces the tracking errors as compared to those in Fig. 8. Table III summarizes the root mean square (RMS) values of the tracking error. We can see that the controller with CLC/MRF reduces the RMS tracking error by more than 67% relative to the controller with CLC only. Moreover, we also verify the performance when a maximum payload of 1 kg is placed onto the positioning stage. The results in Table III show that the RMS tracking error is only increased by 5.6% in the worst case.

V. CONCLUSION

We have studied two resonant compensation techniques and a multi-resonant filter design method for high-bandwidth control of a PZT nanopositioning stage. First, we present the notch filter that is aimed at reducing the resonance peak gain. In contrast, the complex lead compensator is developed by shaping the phase of open-loop system at the resonant frequency. Although the two techniques can damp the resonance mode for reduced vibrations, it is shown that the CLC can provide a much higher closed-loop bandwidth. As a result, the experimental results verify the superiority of the CLC in hysteresis and input disturbance compensation, and periodic trajectory tracking. In order to further reduce the tracking error, we also develop a multi-resonant filter that can provide extra gain attenuations in the sensitivity function

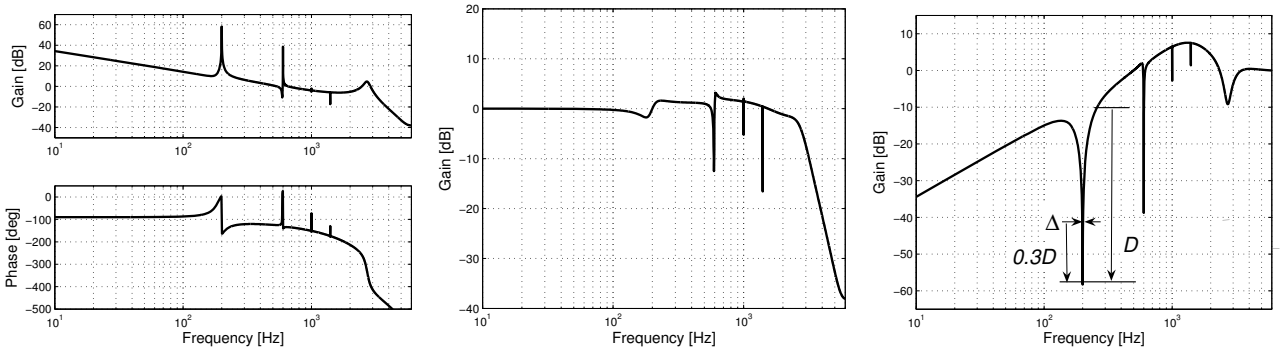

(a) (b) (c)

Fig. 11. Frequency response of the CLC based control system with the add-on MRF. (a) Open-loop FRF $= PCF_{clc}(1+M)$. The MRF does not degrade the stability margin significantly. (b) Closed-loop FRF $= PCF_{clc}(1+M)/(1+PCF_{clc}(1+M))$; (c) Sensitivity FRF $= 1/(1+PCF_{clc}(1+M))$. The gains at the first 4 harmonics of the triangular waveform are further reduced.

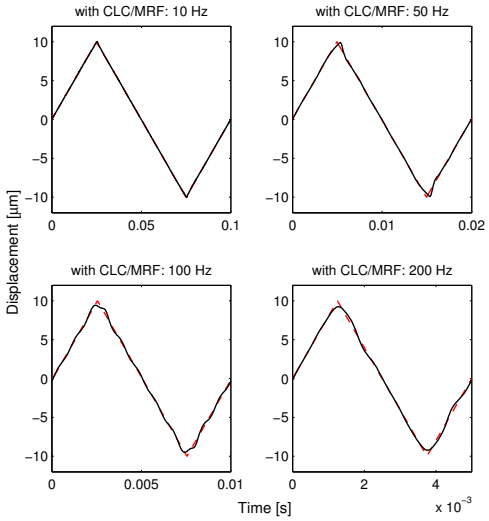

Fig. 12. Triangular waveform tracking with CLC and the add-on MRF. Dashed lines: Triangular reference; Solids lines: Output displacement.

TABLE II

COMPARISON OF STABILITY MARGIN AND CLOSED-LOOP BANDWIDTH

Compensator	Phase margin	Gain margin	Bandwidth
NF	43°@329 Hz	7.04 dB@640 Hz	630 Hz
CLC	58°@527 Hz	7.0 dB@1530 Hz	2512 Hz
CLC/MRF	46°@662 Hz	6.0 dB@1500 Hz	2620 Hz

at specified frequencies. The MRF is of add-on feature for easy implementation and only slightly degrades the stability margin of the baseline control system. The effectiveness of the MRF is also verified by the experimental results.

TABLE III

COMPARISONS OF RMS ERRORS OF THE TRACKING PERFORMANCE

Compensator	10 Hz	50 Hz	100 Hz	200 Hz
NF	0.1494	0.8306	1.8523	3.6720
CLC	0.0968	0.5062	1.0552	2.3687
CLC/MRF	0.0278	0.1651	0.2149	0.2647
CLC/MRF w/payload	0.0286	0.1745	0.1754	0.2733

REFERENCES

[1] G. Binnig, C. Quate, and C. Gerber, "Atomic force microscope," *Phys. Rev. Lett.*, vol. 56, no. 9, pp. 930-933, Mar. 1986.

[2] S. Devasia, E. Eleftheriou, and R. Moheimani, "A survey of control issues in nanopositioning," *IEEE Trans. Control Syst. Technol.*, vol. 15, no. 5, pp. 802-823, Sep. 2007.

[3] K. Leang and S. Devasia, "Feedback-linearized inverse feedforward for creep, hysteresis, and vibration compensation in AFM piezoactuators," *IEEE Trans. Control Syst. Technol.*, vol. 15, no. 5, pp. 927-935, Sep. 2007.

[4] B. Bhikkaji and R. Moheimani, "Integral resonant control of a piezoelectric tube actuator for fast nanoscale positioning," *IEEE/ASME Trans. Mechatron.*, vol. 13, no. 5, pp. 530-537, Oct. 2008.

[5] A. Fleming, "Nanopositioning system with force feedback for high-performance tracking and vibration control," *IEEE/ASME Trans. Mechatron.*, vol. 15, no. 3, pp. 433-447, Jun. 2010.

[6] G. Whitesides and H. Love, "The art of building small," *Scientif. Amer.*, vol. 285, no. 3, pp. 39-47, Sep. 2001.

[7] J. Yi, S. Chang, and T. Shen, "Disturbance-observer-based hysteresis compensation for piezoelectric actuators," *IEEE/ASME Trans. Mechatron.*, vol. 14, no. 4, pp. 456-464, Aug. 2009.

[8] Y. Yong, S. Aphale, and R. Moheimani, "Design, identification, and control of a flexure-Based XY stage for fast nanoscale positioning," *IEEE Trans. Nanotechnol.*, vol. 8, no. 1, pp. 46-54, Jan. 2009.

[9] U. Aridogan, Y. Shan, and K. Leang, "Design and analysis of discrete-time repetitive control for scanning probe microscopes," *J. Dyna. Syst.,Measure., Control*, vol. 131, pp. 061103:1-12, Nov. 2009.

[10] E. Levi, "Complex-curve fitting," *IRE Trans. on Automatic Control*, vol. AC-4, pp. 37-44, 1959.

[11] M. Kobayashi, S. Nakagawa, T. Atsumi, and T. Yamaguchi, "High-bandwidth servo control designs for magnetic disk drives," in *Proc. IEEE/ASME Int. Conf. Adv. Intell. Mechatron.,* 2001, pp. 1124-1129.

[12] W. Messner, M. Bedillion, L. Xia, and D. Karns, "Lead and lag compensators with complex poles and zeros: design formulas for modeling and loop shaping," *IEEE Control Systems Magazine*, vol. 27, no. 1, pp. 44-54, Feb. 2007.

[13] J. Zheng, G. Guo, Y. Wang, and W. E. Wong, "Optimal narrow-band disturbance filter for PZT-actuated head positioning control on a spinstand," *IEEE Trans. Magn.*, vol. 42, no. 11, pp. 3745-3751, Nov. 2006.